NANO LETTERS

Letter

pubs.acs.org/NanoLett

# Greatly Suppressed Shuttle Effect for Improved Lithium Sulfur Battery Performance through Short Chain Intermediates

Na Xu, Tao Qian,* Xuejun Liu, Jie Liu, Yu Chen, and Chenglin Yan*

College of Physics, Optoelectronics and Energy, Suzhou Key Laboratory of Advanced Carbon Materials and Wearable Energy Technology & Collaborative Innovation Center of Suzhou Nano Science and Technology, Soochow University, Suzhou 215006, China

Supporting Information

**ABSTRACT:** The high solubility of long-chain lithium polysulfides and their infamous shuttle effect in lithium sulfur battery lead to rapid capacity fading along with low Coulombic efficiency. To address above issues, we propose a new strategy to suppress the shuttle effect for greatly enhanced lithium sulfur battery performance mainly through the formation of short-chain intermediates during discharging, which allows significant improvements including high capacity retention of 1022 mAh/g with 87% retention for 450 cycles. Without $LiNO_3$-containing electrolytes, the excellent Coulombic efficiency of ~99.5% for more than 500 cycles is obtained, suggesting the greatly suppressed shuttle effect. In situ UV/vis analysis of electrolyte during cycling reveals that the short-chain $Li_2S_2$ and $Li_2S_3$ polysulfides are detected as main intermediates, which are theoretically verified by density functional theory (DFT) calculations. Our strategy may open up a new avenue for practical application of lithium sulfur battery.

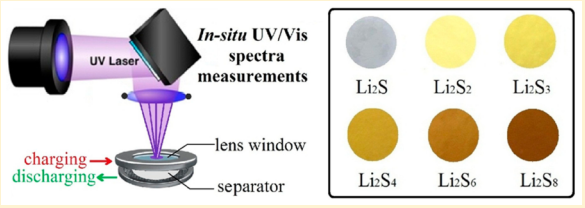


**KEYWORDS:** *Lithium sulfur battery, shuttle effect, in situ UV/vis analysis, short chain intermediates*

As the development of new energy system, electric vehicles and small appliances increases, so do the demands for pursuing advanced rechargeable battery with rapid electrochemical energy conversion and storage.[1,2] Much attention has been paid to sulfur, which acts as one of the most intensely investigated cathode materials in the electrochemical energy storage field with high theoretical capacity and specific energy density.[3,28] The lightweight, high natural abundance, environmental friendliness, low competitive cost, and benign character of sulfur are also promising properties that make it applicable for the application in prospective energy material.[4,29] However, several challenges still exist in the cathode of Li−S batteries (LIBs) that hamper their practical application.[5] Challenges include (1) the incomplete electrochemical conversion, sluggish kinetics, and poor electronic conductivity of bulk sulfur lead to electrochemical inertness in the cathode of LIBs;[6,7] and (2) the high solubility of the long-chain polysulfide's ($Li_2S_x$, $4 < x \leq 8$) reaction intermediates, and the action of their notorious shuttle effect in organic electrolyte, leading to rapid decline in cycle life and capacity.[8] In addition, the shuttle effect arises from the side reaction between the soluble polysulfides and lithium anode, resulting in self-discharge and low Coulombic efficiency, which are regarded as one of the major hurdles for the practical application of LIBs. Various means to overcome these challenges were reported in recent years,[5−7] which are focused on developing carbon coating material accompanied by accelerated fast electron transfer that can physically restrict the shuttle effect of polysulfide, but it still suffers from the problems that the carbon hosts are nonpolar and therefore less efficient in entrapping polar polysulfides.[9−12] In another attempt, the method of enhancing polarity of carbon materials by combining functionalized polar groups[13] with carbon materials or introducing polar metallic oxides ($TiO_2$,[14,30] $Ti_4O_7$,[15,31] $MnO_2$[16,32]) to carbon host have been demonstrated to effectively reduce the shuttle effect. Polar sections can effectively keep lithium polysulfides within the cathode to form relatively strong electrostatic interaction with lithium polysulfides.

Unlike the traditional mechanism of physical absorption, the covalent attachment of sulfur has been demonstrated as more cutting-edge technology to enhance the stability of LIBs. Molecules with various active groups are used to covalently bind sulfur with polymeric materials. Copolymerization of $S_8$ with alkene or its derivative via inverse vulcanization is proposed as a noteworthy strategy to chemically cross-link polymeric sulfur cathode.[17−19] A facile synthesis method was reported by utilizing nitrile groups and $S_8$ to promote dehydrogenation and ring formation.[20] These covalently combining methods have been proved to be hopeful, but challenges still remain in the actual production of such a material occupying poor electronic conductivity and the stabilized mechanism is widely wondered, while it is ambiguous to date. In addition, the use of $LiNO_3$ additive could be an effective way to protect lithium metal anodes associated with dissolved polysulfide species. However, as a strong oxidizing

**Received:** November 4, 2016
**Revised:** December 9, 2016
**Published:** December 15, 2016





DOI: 10.1021/acs.nanolett.6b04610
Nano Lett. 2017, 17, 538−543

chemical, the chemical $LiNO_3$ explosive could have safety issues especially at high working temperatures.

To address above issues, we present a novel S−S bond breakage mechanism toward highly stable and high Coulombic efficiency sulfur cathodes without $LiNO_3$ additive by the covalent attachment of sulfur to the sulfydryl-functionalized graphene nanosheets. Specifically, cysteamine is chosen as a bridge due to its unique structure with amine and sulfydryl groups to covalently combine sulfur copolymer with graphene nanosheets. The covalently stabilized sulfur on sulfydryl functionalized reduced graphene oxide (denoted as S-GSH) enables us to achieve a high capacity retention of 87% for 450 cycles with a capacity of 1022 mAh/g. Remarkably, without using $LiNO_3$ additive electrolyte, the Coulombic efficiency reaches over 99.8% for more than 500 cycles, suggesting the great potential for highly stable Li−S battery system without $LiNO_3$-containg electrolyte. In order to get an insight into the new lithium sulfur reaction mechanism, we use in situ UV/vis spectroscopy to study the interaction between lithium polysulfides and UV/vis radiation. The polysulfides could be qualitatively determined from the spectra that was obtained from cathode electrolyte with chemically synthesized stoichiometric mixtures of polysulfides. Basing on the UV/vis reflection wavelengths obtained from different polysulfide concentrations, the wavelength "standards" were obtained. In the light of the measured "standards", S-GSH cathode only shows up short-chain lithium sulfides during discharge, and no lithium dendrites are produced, which mean that the functionalized cathodes do have effect on suppressing the shuttle effect. Moreover, density-functional theory (DFT) calculation is used to verify the conclusion deduced from UV/vis tests. The deep going mechanism analysis sets novel trends and offers ideas for avenues to get further research to facilitate Li−S battery technologies.

Two steps are involved to compound the S-GSH. First, by nucleophilic attack to b-carbon and epoxy carbon of hydroxyl groups on graphene oxide (GO) surface at 90 °C, cysteamine are grafted onto the GO.[21] With the elimination of oxygen containing moieties, electrically insulating GO is synchronously reduced to conductive rGO accompany. The interlinkage of rGO nanosheets is controlled by inhibiting exactly over the reaction temperature and precursor concentration in order to facilitate the following sulfur loading. Second, impregnating sulfur into sulfydryl-functionalized rGO (GSH) and ring-opening polymerization of elemental sulfur with grafted sulfydryl groups of GSH via free radical copolymerization follows the synthetic scheme given in Figure 1, and detailed

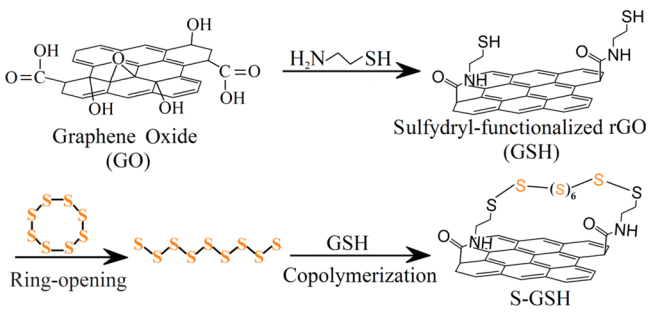


**Figure 1.** Copolymerization of $S_8$ with GSH. Synthetic scheme for the grafting of cysteamine with graphene oxide, and the copolymerization of $S_8$ with sulfydryl to form chemically stable sulfur copolymers.

procedures are provided in the methods (Supporting Information). Scanning electron microscopy (SEM) images (Figure S1) reveal the two-dimensional lamellar structure of GSH. As shown in Figure S1B, energy-dispersive X-ray spectroscopy (EDAX) is used for elemental mapping of the selected area, which indicates that all of the elements (sulfur, nitrogen, carbon) are uniformly distributed over the GSH nanosheets.

The covalent binding of cysteamine to rGO nanosheets can be clearly evidenced by X-ray photoelectron spectroscopy, which is employed to detect element changes before and after the reduction (Figure S2A). The presence of sulfur and nitrogen signals at 164.2[16] and 400.2 eV,[9] respectively, as well as the decrease of oxygen peak intensity suggest that the sulfydryl group is successfully grafted onto the rGO. After covalently binding sulfur, the peak intensity of sulfur is increased. Moreover, Raman spectra (Figure S2B) of GO and GSH both exhibit the band at around 1335 $cm^{-1}$, which is assigned to the disordered graphitic lattice or $sp^3$-rich phase,[22] and the band at around 1595 $cm^{-1}$, which is ascribed to $sp^2$-C atoms pairs with in-plane bond stretching motion.[23] The $I_D/I_G$ ratio shows a considerable enhancement from 1.19 for GO to 1.23 for GSH, suggesting the introduction of additional defects of graphene basal plane by molecular cysteamine.

The electrochemical performance of Li−S battery with S-GSH cathode is evaluated using CR2025 coin batteries. The electrochemical kinetic process of the S-GSH cathode is first studied with cyclic voltammetry (CV) (Figure S3). When the voltage is swept between 1.5 and 2.8 V, two obvious cathodic peaks can be seen with onset potentials at approximately 1.83 and 2.15 V. During the following anodic scan, the peak at 2.54 V is attributed to the oxidation of lithium sulfides to sulfur. After the first scan, two reduction peaks are observed at around 2.23 and 1.91 V, which correspond to the multistep reduction mechanism of the covalent binding sulfur.

Figure S6A shows the galvanostatic charge/discharge profile exhibits a specific capacity of 1108 mAh/g at the initial cycle. During the following cycles, the capacity can keep stable at ∼1036 mAh/g. The comparison results of the discharge profiles between the second and 150th cycles reveal negligible changes in both the shape and specific capacity with a Coulombic efficiency approaching 99%. The excellent cycling performance of S-GSH at a rate of 1 C is in striking contrast to the poor discharge capacity of 438 mAh/g and poor capacity retention of 48% for the S-rGO cathode (Figure 2B). It was found that the initial charge−discharge efficiency of the S-GSH (96.3%) is much higher than that for S-rGO (90.3%) at a constant 1 C rate, which is due to the reduced irreversible capacity loss by sulfydryl functionalization. Figure S5A shows the effect of current density on performance of Li−S battery with S-GSH cathode. The profiles show increasingly shortened charge−discharge plateaus with increasing rate due to the electrode polarization.[24] At a high rate of 2 C, a high capacity of ∼952 mAh/g and stable cycle performance can be still retained. The initial capacities are 1114, 1032, and 985 mAh/g, and the corresponding capacity retentions are 93.8%, 87.5%, and 84.8% after 200 cycles (Figure S5B). The cycling life of S-GSH battery can be broadened to 450 cycles simultaneously with high capacity retention of 87% and retain a capacity of 857 mAh/g (Figure 2A). The cycling resistance is investigated to illustrate the cycling stability by electrochemical impedance spectroscopy (EIS). As shown in Figure S7, the resistance becomes quite stable after activation at the first cycle, and a charge transfer


DOI: 10.1021/acs.nanolett.6b04610
Nano Lett. 2017, 17, 538−543

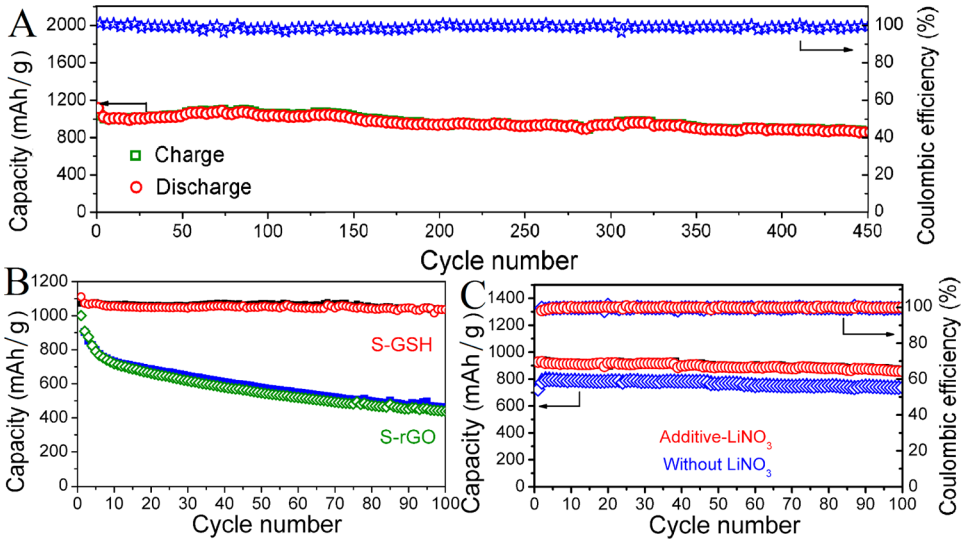


**Figure 2.** (A) Long-term cyclability of S-GSH cathode at a current density of 1675 mA/g. (B) Cycling performance of S-GSH and S-rGO cathodes at a current density of 1 C. (C) Cycling performance and Coulombic efficiencies of S-GSH electrodes at 1 C with two different electrolytes.

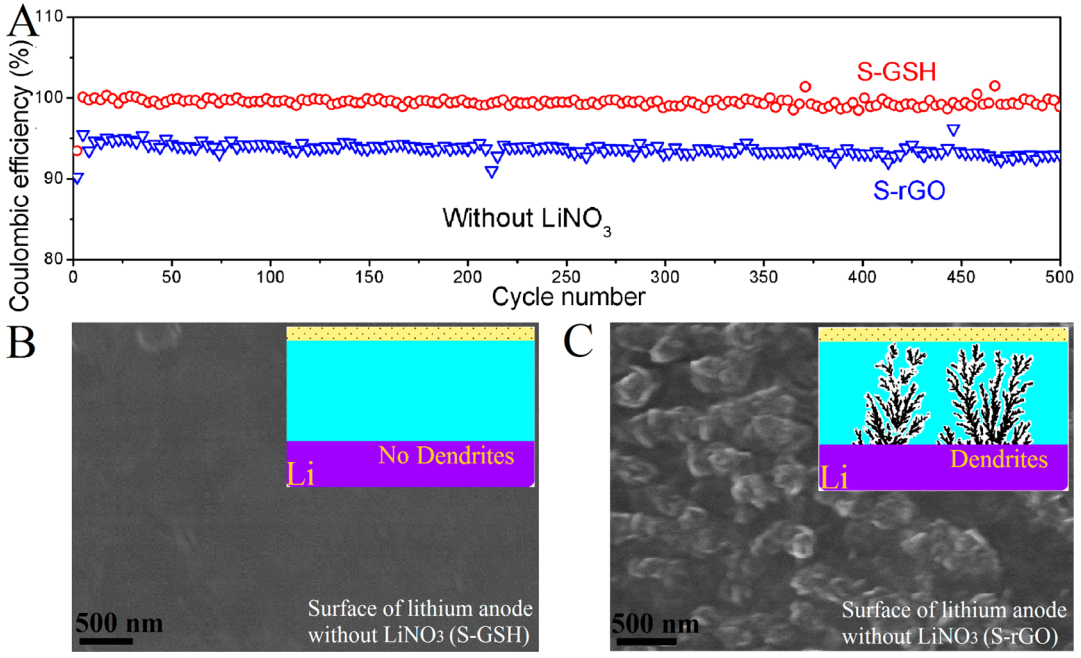


**Figure 3.** (A) Coulombic efficiencies of S-GSH and S-rGO cathodes at a current density of 1675 mA/g. (B,C) SEM images of the lithium anode surface in the electrolyte without $LiNO_3$ after 100 cycles at a current rate of 0.5 C with S-GSH and S-rGO cathodes, respectively.

resistance of less than 21.2 Ω is achieved after 100 cycles (Table S2). The stable and small ohmic resistance, as well as charge transfer resistance, vary slightly at the recharge state, implying highly reversible structure evolution of the S-GSH cathode during cycling processes. The performance improvements according from specific capacity, rate capability, and cycling life clearly validate that the sulfydryl functionalization plays a critical role in performance enhancement of S-GSH cathode.

Typical lithium sulfur batteries without lithium nitrate ($LiNO_3$) as additive to ether-based electrolyte may lead to large amount production of long-chain lithium polysulfides (LiPSs) and the growth of lithium dendrites.[33,34] However, the dissolution character of polysulfides also leads to the shuttle effect, where LCPs diffuse onto the lithium anode surface and reduced to short-chain polysulfides (SCPs). This parasitical course takes place unceasingly, creating "shuttle" phenomena internally, which decreases the active mass and also obviously reduces the Coulombic efficiency. In addition, there is a potential explosive dangerous for the use of strong oxidizing $LiNO_3$ additive in LIBs. Therefore, we develop the new Li−S battery system without using $LiNO_3$ to achieve highly stable performance. As shown in Figure 2C, S-GSH cathodes are tested in the electrolyte with 1 wt % $LiNO_3$ (~0.15 M) at a rate of 1 C, the specific capacity of 858 mAh/g with a capacity retention of 92.6% can be obtained. When using $LiNO_3$-free electrolyte, the S-GSH cathode can still deliver a specific capacity of 740 mAh/g after 100 cycles. Remarkably, S-GSH battery using electrolyte without any additives can operate without failure for more than 100 cycles with a Coulombic



DOI: 10.1021/acs.nanolett.6b04610
Nano Lett. 2017, 17, 538−543

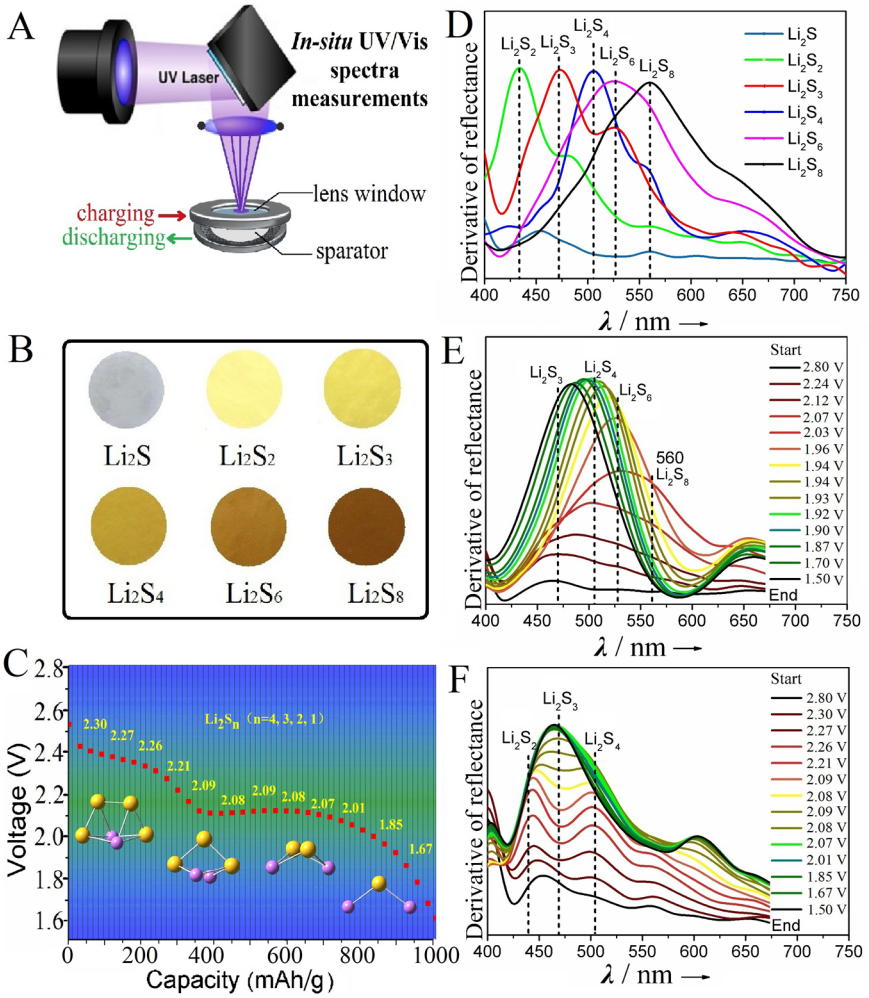


**Figure 4.** In situ UV/vis spectra measured during the first discharge of lithium sulfur battery with 1 M LiTFSI and 1 wt % $LiNO_3$ in 1,3-dioxolane and 1,2-dimethoxyethane (volume ratio 1:1) electrolyte. (A) The cell configuration with a sealed glass window for in situ UV/vis investigation. (B) Photographs of six different catholyte solutions in 1 M LiTFSI and 1 wt % $LiNO_3$ in 1,3-dioxolane and 1,2-dimethoxyethane (volume ratio 1:1) electrolyte (the stoichiometric ratio between lithium and sulfur is presented at the bottom of each picture column). (C) The selected discharge voltages were applied for in situ UV/vis measurements. (D) The corresponding UV/vis spectra first-order derivative curves of different stoichiometric mixtures. The corresponding UV/vis spectra first-order derivative curves of (E) S-rGO and (F) S-GSH electrodes at a current rate of C/3, respectively.

efficiency as high as 98.5% at a rate of 450 mA/g (Figure S6B). The high Coulombic efficiency of ~99.5% is also remained at a high rate of 1675 mA/g for more than 500 cycles (Figure 3A). However, the Coulombic efficiency of S-rGO cathodes drops from 95.5% to 93.5% after 500 cycles. It reveals that the sulfydryl group can greatly improve the Coulombic efficiency to alleviate the shuttle effect caused by lithium polysulfides. We also examine the morphology of lithium anodes for both Li/S-GSH and Li/S-rGO cells after 100 cycles in the electrolyte without $LiNO_3$ as additives. In Li/S-GSH cell, a very dense and uniform SEI layer can be observed on the anode, and the top surface of the lithium still exhibit uniform morphology without growth of lithium dendrites after 100 cycles (Figures 3B and S15A). In contrast, uneven growth of sharp, thin and fiber-like lithium dendrites is clearly observed after 100 cycles when using S-rGO cathode (Figures 3C and S15B). This structure not only contributes to a higher potential of the stripping dead lithium but also threatens the safety of battery by puncturing the separator. As a result, sulfydryl group can effectively avoid the shuttle effect during cycling.

To gain an insight into the reaction mechanism of the interaction between sulfydryl group and the sulfur copolymer, in situ UV/vis spectroscopy is performed by analyzing the component transformation occurred in the electrolyte during the cycle process. Various lithium polysulfides can be qualitatively determined with in situ UV/vis spectroscopy. Moreover, long- and short-chain polysulfides can be clearly distinguished.[25,26] Six different samples with varied ratios of lithium sulfide and sulfur were prepared, which are denoted according to the proportion of the added amount (i.e., $Li_2S_x$, in which $x$ = 2−8). When the polysulfides are dissolved in 1 M LiTFSI in 1,2-dimethoxyethane and 1,3-dioxolane with a volume ratio of 1:1 to be used as electrolyte, the color of electrolyte changed from transparency to dark red (Figure 4B). It should be noted that the absorption wavelength of the measure reflectance is a function of the state of the battery in UV/vis spectrometer, such as the type of cathode composite, and the quantity and wettability of the electrolyte used in the battery. Hence, we should normalize all measured spectra for comparison. As shown in Figure 4D, it is found that the derivatives for long-chain polysulfides at $\lambda$ = 560 and 530 nm


DOI: 10.1021/acs.nanolett.6b04610
Nano Lett. 2017, 17, 538−543

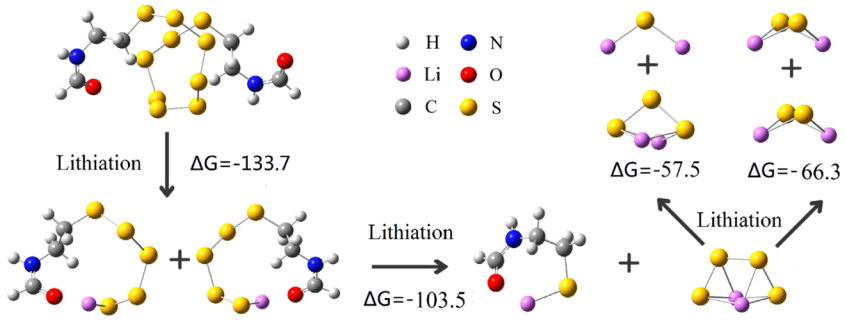


**Figure 5.** Illustration for the three steps of Li insertion by DFT calculations. All the models are shown in the most stable configuration. In the models, the carbon (C), hydrogen (H), nitrogen (N), sulfur (S), oxygen (O), and lithium (Li) elements are displayed as spheres in gray, white, blue, yellow, red, and pink, respectively.

correspond to the $Li_2S_8$ and $Li_2S_6$ during initial discharging, respectively. In contrast, the derivatives showing up at $\lambda$ = 505, 470, and 435 nm for short-chain polysulfides are attributed to the formation of $Li_2S_4$, $Li_2S_3$, and $Li_2S_2$ during further discharging, respectively. During discharging process, the derivative peaks of S-rGO cathode shifts from 560 to 480 nm wavelengths continuously as can be seen in Figure 4E, and the mainly generated polysulfide intermediates for S-rGO cathode are $Li_2S_8$, $Li_2S_6$, $Li_2S_4$, and $Li_2S_3$. During charging, the peak gradually shifts from short wavelengths to the long wavelengths when the cell is charging from 1.5 to 2.8 V, corresponding to an increase in the chain length of polysulfides with the extraction of $Li^+$ (Figure S9C). Both $Li_2S_6$ and $Li_2S_8$ as soluble lithium polysulfide would dissolve in electrolyte during charge−discharge progress, which results in the wastage of active materials. Differently, as for S-GSH, the derivative peaks appear at 435 and 505 nm first, and finally converge to 470 nm. With the proceed of the discharge process, $Li_2S_2$ and $Li_2S_4$ are mainly generated at the beginning, then with more $Li^+$ implanted, $Li_2S_4$ transforms to $Li_2S_3$, while $Li_2S_2$ transforms to $Li_2S$. Since $Li_2S$ shows no detected derivative peak, both derivative peaks at 435 (corresponding to $L_2S_2$) and 505 nm (arising from $L_2S_4$) disappear, and the only remaining derivative peak from $Li_2S_3$ is observed at 470 nm (Figure 4F). During charging, almost no derivative peaks of long-chain polysulfide show up in S-GSH cathode (Figure S9E), but a continuous shift from short to long wavelengths can be observed for S-rGO cathode (Figure S9C). It is concluded that the S−S bond breakage mechanism for S-GSH cathodes is mainly based on the formation of short-chain intermediates during discharging.

In order to further verify which kind of LiPSs mainly existed during discharging, cells were disassembled at the discharge states of 2.27 and 2.10 V. As shown in Figure S17, the trace of the dissolved LiPSs on the separator from the S-rGO cell at a discharge state of 2.27 V shows conspicuous red color in a large area, implying a large amount of long-chain LiPSs were generated. With further discharging to 2.10 V, the color of separator turns to yellow, indicating that the long-chain LiPSs transform to short-chain LiPSs. For comparison, the trace of the dissolved LiPSs on the separator from the S-GSH cells at the discharge states of 2.27 and 2.10 V both show inconspicuous yellow color in a small area, illustrating the effective restriction of generation of long chain LiPSs in the S-rGO cathodes during discharging process. The above experiments indicate that sulfydryl groups have prominent effect on immobilizing sulfur and suppressing the generation of long-chain polysulfides during both charging and discharging process.

To verify the observed mechanism, we systematically investigate the intermediates during the lithiation process by DFT calculations. The physically weakened adhesive force of sulfur to the carbon surface consequentially causes the separation and detachment of electroactive material from carbon matrix, resulting in bad performance of most sulfur−carbon composites. After sulfydryl functionalization, the ring-opened $S_8$ is covalently stabilized on the graphene host by chemical bonding, which is much stronger than physical adhesion. To demonstrate that short-chain polysulfides are the main intermediate products during discharging, we presume the most likely pathway with three steps as shown in Figure 5. The results suggest that the initial S−S bond breakage takes place at the middle of the polymerized sulfur chain, which releases 133.7 kcal/mol Gibbs free energy with the insertion of two lithium ions. The following activation barrier is further calculated with the insertion of another two lithium ions, and the results show that $Li_2S_4$ is the most possible intermediate to be produced with the lowest Gibbs free energy. With the procession of the subsequent lithiation, the generated $Li_2S_4$ would split into $Li_2S$ and $Li_2S_3$ or two moles of $Li_2S_2$, with Gibbs free energy changes of −57.5 or −66.3 kcal/mol, respectively. Thus, with abundant insertion of $Li^+$, the finally generated lithium polysulfides are $Li_2S$, $Li_2S_2$, and $Li_2S_3$ (for details, there are different ways to break the sulfur chain with the insertion of lithium ions, and the calculated energy consumption changes are shown in Figures S10−12). In addition, the strong appetency of $Li_2S$ to the carbon matrix is fairly important to maintain the electrical contact and active mass of the composite after full discharge of electroactive material. To understand the reciprocity between the GSH and the discharge products, further DFT calculations are performed where single layer graphene is taken as model substrate on behalf of carbon surface, and $Li_2S$ represents the lithium polysulfide during discharging process. This method may not provide a categorical quantification of the binding energy between GSH and the lithium sulfide species, but offer a qualitative comprehending on interfacial effect. The corresponding binding energy between carbon surface and $Li_2S$ is 0.26 eV (Figure S13A), which is smaller than that of elemental sulfur (0.79 eV).[27] The attenuation of sulfur absorbs to the carbon surface and the enhanced ionic binding between the lithium sulfide mixtures, giving rise to self-aggregation and the detachment of lithium polysulfide species from carbon surface during further discharge process. After cysteamine functionalization, $Li_2S$ binds to SH moieties by connecting to sulfur of the sulfydryl group with binding energy of 1.51 eV (Figure S13B). As a consequence, the separation and detachment of lithium


DOI: 10.1021/acs.nanolett.6b04610
Nano Lett. 2017, 17, 538−543

sulfides from the grafted $S_8$ linear chain could be efficaciously repressive to accomplish good stability for long-range charge−discharge cycle performance.

In conclusion, we present a new strategy to suppress the shuttle effect based on the formation of short chain polysulfide discharge products by the covalent attachment of sulfur to the sulfydryl-functionalized graphene nanosheets. With this new strategy, the sulfydryl-functionalized cathodes do have effect on suppressing the long-chain lithium sulfide and can effectively avoid the shuttle effect. In situ UV/vis spectra confirm that no long-chain polysulfides show up throughout the charge−discharge process. A detailed density-functional theory (DFT) computation further verifies that with abundant insertion of $Li^+$ the finally formed lithium polysulfides are $Li_2S$, $Li_2S_2$, and $Li_2S_3$. The benefits of the strategy are also demonstrated in lithium−sulfur batteries where they are shown to promote to a high Coulombic efficiency of ~99.5% without using $LiNO_3$ additive, which is typically used in conventional Li−S battery to protect the lithium metal anode from reacting with dissolved polysulfides. This novel mechanism may open the way to a departure from traditional cathode design for LIBs based on functionalized carbon materials and could animate further studies on the essence of the polysulfide−support interaction.

## ■ ASSOCIATED CONTENT

### Supporting Information

The Supporting Information is available free of charge on the ACS Publications website at DOI: 10.1021/acs.nanolett.6b04610.

Experimental section, TEM images, elemental analysis of different samples, CV curves, *in situ* UV/vis spectra of electrodes during charging, XPS spectra and electrochemical properties for different samples (PDF)

## ■ AUTHOR INFORMATION


### Corresponding Authors

*E-mail: tqian@suda.edu.cn.

*E-mail: c.yan@suda.edu.cn.

### ORCID

Yu Chen: 0000-0001-9669-2475

Chenglin Yan: 0000-0003-4467-9441


### Notes

The authors declare no competing financial interest.

## ■ ACKNOWLEDGMENTS

We acknowledge the support from the "Thousand Talents Program", the National Natural Science Foundation of China (no. 51402202 and 51622208), and the Priority Academic Program Development of Jiangsu Higher Education Institutions (PAPD).

## ■ REFERENCES


(1) Armand, M.; Tarascon, J. M. *Nature* **2008**, *451*, 652−657.

(2) Qie, L.; Manthiram, A. *Adv. Mater.* **2015**, *27*, 1694−1700.

(3) Yang, Y.; Zheng, G. Y.; Cui, Y. *Chem. Soc. Rev.* **2013**, *42*, 3018−3032.

(4) Bruce, P. G.; Freunberger, S. A.; Hardwick, L. J.; Tarascon, J. M. *Nat. Mater.* **2012**, *11*, 19.

(5) Zhang, Z. W.; Li, Z. Q.; Hao, F. B.; Wang, X. K.; Li, Q.; Qi, Y. X.; Fan, R. H.; Yin, L. W. *Adv. Funct. Mater.* **2014**, *24*, 2500−2509.

(6) Kim, J.; Lee, D. J.; Jung, H.-G.; Sun, Y.-K.; Hassoun, J.; Scrosati, B. *Adv. Funct. Mater.* **2013**, *23*, 1076−1080.

(7) Yang, Y.; McDowell, M. T.; Jackson, A.; Cha, J. J.; Hong, S. S.; Cui, Y. *Nano Lett.* **2010**, *10*, 1486−1491.

(8) Zhang, C. F.; Wu, H. B.; Yuan, C. Z.; Guo, Z. P.; Lou, X. W. *Angew. Chem., Int. Ed.* **2012**, *51*, 9592−9595.

(9) Pang, Q.; Tang, J. T.; Huang, H.; Liang, X.; Hart, C.; Tam, K. C.; Nazar, L. F. *Adv. Mater.* **2015**, *27*, 6021−6028.

(10) He, G.; Evers, S.; Liang, X.; Cuisinier, M.; Garsuch, A.; Nazar, L. F. *ACS Nano* **2013**, *12*, 10920−10930.

(11) Ji, L. W.; Rao, M. M.; Aloni, S.; Wang, L.; Cairns, E. J.; Zhang, Y. G. *Energy Environ. Sci.* **2011**, *4*, 5053−5059.

(12) Ji, X.; Evers, S.; Black, R.; Nazar, L. F. *Nat. Commun.* **2011**, *2*, 325−331.

(13) Ma, L.; Zhuang, H. L.; Wei, S. Y.; Hendrickson, K. E.; Kim, M. S.; Cohn, G.; Hennig, R. G.; Archer, L. A. *ACS Nano* **2016**, *10*, 1050−1059.

(14) Liang, Z.; Zheng, G.; Li, W.; Seh, Z. W.; Yao, H.; Yan, K.; Kong, D.; Cui, Y. *ACS Nano* **2014**, *8*, 5249−5256.

(15) Pang, Q.; Kundu, D.; Cuisinier, M.; Nazar, L. F. *Nat. Commun.* **2014**, *5*, 4759.

(16) Liang, X.; Hart, C.; Pang, Q.; Garsuch, A.; Weiss, T.; Nazar, L. F. *Nat. Commun.* **2015**, *6*, 5682.

(17) Chung, W. J.; Griebel, J. J.; Kim, E. T.; Yoon, H.; Simmonds, A. G.; Ji, H. J.; Dirlam, P. T.; Glass, R. S.; Wie, J. J.; Nguyen, N. A.; Guralnick, B. W.; Park, J.; Somogyi, Á.; Theato, P.; Mackay, M. E.; Sung, Y. E.; Char, K.; Pyun, J. *Nat. Chem.* **2013**, *5*, 518−524.

(18) Griebel, J. J.; Li, G.; Glass, R. S.; Char, K.; Pyun, J. *J. Polym. Sci., Part A: Polym. Chem.* **2015**, *53*, 173−177.

(19) Simmonds, A. G.; Griebel, J. J.; Park, J.; Kim, K. R.; Chung, W. J.; Oleshko, V. P.; Kim, J.; Kim, E. T.; Glass, R. S.; Soles, C. L.; Sung, Y. E.; Char, K.; Pyun, J. *ACS Macro Lett.* **2014**, *3*, 229−232.

(20) Wei, S. Y.; Ma, L.; Hendrickson, K. E.; Tu, Z. Y.; Archer, L. A. *J. Am. Chem. Soc.* **2015**, *137*, 12143−12152.

(21) Hu, H.; Zhao, Z.; Wan, W.; Gogotsi, Y.; Qiu, J. *Adv. Mater.* **2013**, *25*, 2219−2223.

(22) Sevilla, M.; Fuertes, A. B. *ACS Nano* **2014**, *8*, 5069−5078.

(23) Sadezky, A.; Muckenhuber, H.; Grothe, H.; Niessner, R.; Poschl, U. *Carbon* **2005**, *43*, 1731−1742.

(24) Ji, X.; Lee, K. T.; Nazar, L. F. *Nat. Mater.* **2009**, *8*, 500−506.

(25) Patel, M. U. M.; Dominko, R. *ChemSusChem* **2014**, *7*, 2167−2175.

(26) Patel, M. U. M.; Cakan, R. D.; Morcrette, M.; Tarascon, J. M.; Gaberscek, M.; Dominko, R. *ChemSusChem* **2013**, *6*, 1177−1181.

(27) Zheng, G. Y.; Zhang, Q. F.; Cha, J. J.; Yang, Y.; Li, W. Y.; Seh, Z. W.; Cui, Y. *Nano Lett.* **2013**, *13*, 1265−1270.

(28) Cheng, X. B.; Peng, H. J.; Huang, J. Q.; Zhang, R.; Zhao, C. Z.; Zhang, Q. *ACS Nano* **2015**, *9*, 6373−6382.

(29) Zhao, C. Z.; Cheng, X. B.; Zhang, R.; Peng, H. J.; Huang, J. Q.; Rui, R.; Huang, Z. H.; Wei, F.; Zhang, Q. *Energy Storage Mater.* **2016**, *3*, 77−84.

(30) Tao, X.; Wang, J.; Ying, Z.; Cai, Q.; Zheng, G.; Gan, Y.; Huang, H.; Xia, Y.; Liang, C.; Zhang, W.; Cui, Y. *Nano Lett.* **2014**, *14*, 5288−5294.

(31) Li, Z.; Zhang, J.; Lou, X. W. *Angew. Chem., Int. Ed.* **2015**, *54*, 12886−12890.

(32) Tao, X.; Wang, J.; Liu, C.; Wang, H.; Yao, H.; Zheng, G.; Seh, Z. W.; Cai, Q.; Li, W.; Zhou, G.; Zu, C.; Cui, Y. *Nat. Commun.* **2016**, *7*, 11203.

(33) Cheng, X. B.; Zhang, R.; Zhao, C. Z.; Wei, F.; Zhang, J. G.; Zhang, Q. *Adv. Sci.* **2016**, *3*, 1500213.

(34) Wang, D.; Zhang, W.; Zheng, W. T.; Cui, X. Q.; Rojo, T.; Zhang, Q. *Adv. Sci.* **2016**, 1600168.




DOI: 10.1021/acs.nanolett.6b04610
*Nano Lett.* 2017, 17, 538−543